Cell PRESS
Open ACCESS

Cell Reports
Report

The Transcription Factor IRF3 Triggers "Defensive Suicide" Necrosis in Response to Viral and Bacterial Pathogens

Nelson C. Di Paolo,[1] Konstantin Doronin,[1,3] Lisa K. Baldwin,[1] Thalia Papayannopoulou,[2] and Dmitry M. Shayakhmetov[1,*]
[1]Division of Medical Genetics
[2]Division of Hematology, Department of Medicine
University of Washington, Seattle, WA 98195, USA
[3]Present address: Department of Molecular Microbiology and Immunology, St. Louis University, St. Louis, MO 63104, USA
*Correspondence: dshax@uw.edu
http://dx.doi.org/10.1016/j.celrep.2013.05.025

SUMMARY

Although molecular components that execute noninflammatory apoptotic cell death are well defined, molecular pathways that trigger necrotic cell death remain poorly characterized. Here, we show that in response to infection with adenovirus or *Listeria monocytogenes*, macrophages in vivo undergo rapid proinflammatory necrotic death that is controlled by interferon-regulatory factor 3 (IRF3). The transcriptional activity of IRF3 is, surprisingly, not required for the induction of necrosis, and it proceeds normally in mice deficient in all known regulators of necrotic death or IRF3 activation, including RIPK3, caspases 1, 8, or 11, STING, and IPS1/MAVS. Although *L. monocytogenes* triggers necrosis to promote the infection, IRF3-dependent necrosis is required for reducing pathogen burden in the models of disseminated infection with adenovirus. Therefore, our studies implicate IRF3 as a principal and nonredundant component of a physiologically regulated necrotic cell-death pathway that operates as an effective innate immune mechanism of host protection against disseminated virus infection.

INTRODUCTION

Physiologically regulated cell death is a fundamental process in multicellular organisms that is critical for host survival. Although molecular components that execute noninflammatory apoptotic cell death are well defined, molecular pathways that trigger regulated proinflammatory necrotic cell death remain poorly characterized. In response to pathogens, damage, or stress, cells can undergo a caspase-1-dependent proinflammatory type of cell death called pyroptosis (Bergsbaken et al., 2009). Under the conditions when apoptotic caspases are blocked, in response to pleiotropic cytokine TNF-α or Fas ligand, cells can undergo RIPK1-RIPK3-dependent necroptosis (Kaczmarek et al., 2013). Cells dying via caspase-1-dependent pyroptosis and RIPK1-RIPK3-dependent necroptosis exhibit similar morphological changes that include lack of chromatin condensation and the loss of plasma membrane integrity.

Human adenovirus (HAdv) is a common human pathogen, and for immunocompromised individuals, HAdv infections can be lethal (Kojaoghlanian et al., 2003). Accumulated data using wild-type HAdv species and HAdv-based vectors in preclinical studies and clinical gene therapy trials demonstrate that virus particles are efficiently cleared from the blood by resident liver macrophage Kupffer cells (Lieber et al., 1997; Morral et al., 2002). However, after interaction with the virus, Kupffer cells undergo rapid death (Manickan et al., 2006), and molecular pathways triggering this response and its physiological relevance remain undefined.

Here, we show that interferon-regulatory factor 3 (IRF3) is a principal and nonredundant factor that triggers rapid necrotic macrophage cell death in vivo in response to disseminated infections with adenovirus or *Listeria monocytogenes*. The activation of this IRF3-dependent cell death is associated with the loss of plasma membrane integrity within minutes after the pathogen challenge and, remarkably, does not require IRF3-dependent gene expression. Although *L. monocytogenes* triggers IRF3-dependent necrosis to promote the infection, macrophage necrosis is required for reducing pathogen burden in the models of disseminated infection with adenovirus. Collectively, our studies reveal a physiologically regulated necrotic cell-death pathway that operates as an effective innate immune mechanism of host protection against disseminated virus infection.

RESULTS

HAdv Triggers a Necrotic Type of Macrophage Death In Vivo, Independently of Caspase-1, Caspase-8, Caspase-11, and RIPK3

To classify the type of death that Kupffer cells undergo after exposure to HAdv (Galluzzi et al., 2012), we utilized an all-in vivo approach and challenged mice deficient in principal mediators of the known specific regulated cell-death mechanisms and immune pathways with the virus (Table S1). Intravenous injection of wild-type HAdv into wild-type mice resulted in efficient trapping of virus particles by $CD68^+$ resident liver macrophages (Figure 1A). Furthermore, subsequent administration of mice with membrane-impermeable dye propidium iodide (PI) revealed

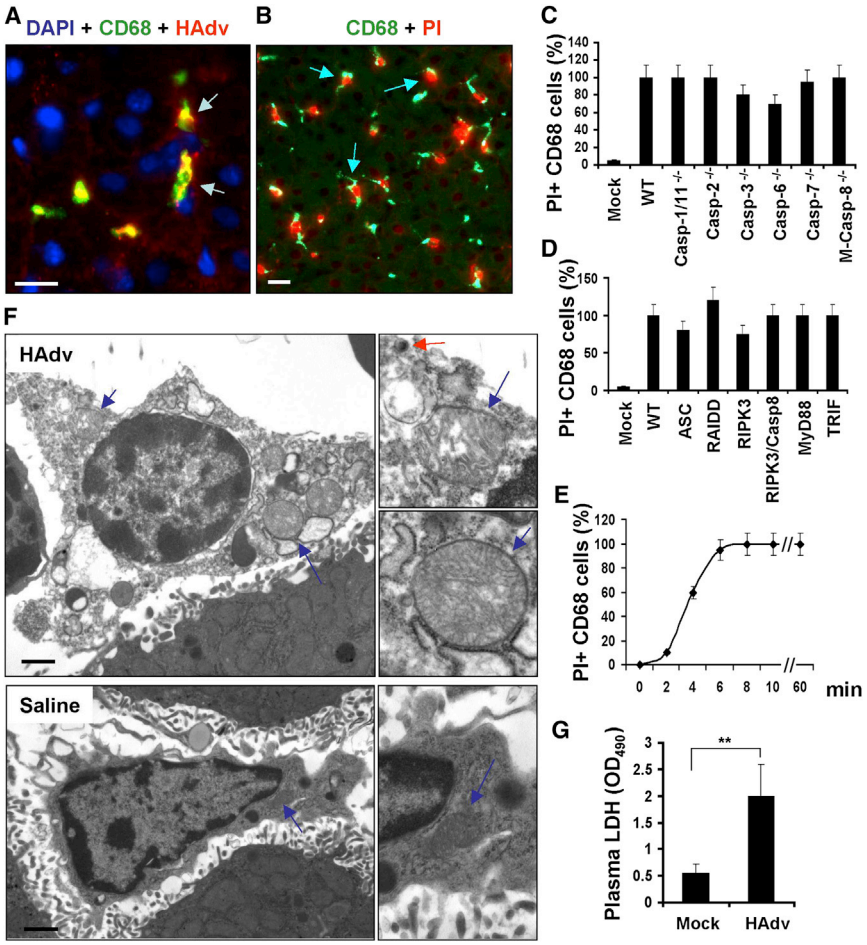

Figure 1. HAdv Triggers a Necrotic Type of Macrophage Death In Vivo, Independently of Caspase-1, Caspase-8, and RIPK3

(A) Confocal microscopy analysis of HAdv particle distribution in liver parenchyma revealed accumulation of the virus (red, indicated by arrows) in CD68$^+$ resident macrophages (green). Cell nuclei were strained with DAPI (blue) (n = 8). Scale bar, 10 μm.

(B) CD68$^+$ liver macrophages (green) become PI permeable (red, indicated by arrows) after interaction with HAdv (n = 8). Scale bar, 10 μm.

(C and D) The percentage of PI-permeable CD68$^+$ cells in the liver parenchyma of indicated gene-deficient mice 60 min after challenge with HAdv. Error bars represent SD of the mean. M-Casp-8$^{-/-}$, mice with macrophage-specific ablation of caspase-8 (n = 8). Casp, caspase.

(E) Kinetics of plasma membrane integrity loss by CD68$^+$ macrophages in the livers of wild-type mice after challenge with HAdv (n = 5).

(F) Electron microscopy analysis of ultrastructural changes in liver macrophages 15 min after challenge with HAdv in vivo. Right panels show the high-power images of mitochondria (blue arrows) and the virus (red arrow). Scale bars, 2 μm (n = 5).

(G) Plasma LDH levels in mice mock infected with saline or infected with HAdv 30 min postinfection (n = 5). **$p < 0.01$.

See also Figure S1.

that nuclei of all CD68$^+$ cells were stained PI positive, demonstrating that these cells have lost their plasma membrane integrity (Figures 1B and S1A). Mice deficient in inflammatory and apoptotic caspases demonstrated no reduction in sensitivity of liver macrophages to HAdv challenge (Figure 1C). HAdv administration to mice deficient in various inflammatory cytokines, Toll-like receptors, cathepsins B, L, and S, superoxide-producing NADPH oxidase components p47^{Phox} and gp91^{Phox}, proapoptotic proteins BAK and BAX, or mitochondrial cyclophilin D (*Ppif*$^{-/-}$) showed a lack of resistance of liver macrophages to the virus (Figures S1C–S1F). Furthermore, HAdv administration to mice deficient in key mediators of pyronecrosis (ASC-deficient *Pycard*$^{-/-}$), necroptosis (*Ripk3*$^{-/-}$ and *Casp8*$^{-/-}$/*Ripk3*$^{-/-}$), stress response PIDDosome (RAIDD-deficient mice, *Cradd*$^{-/-}$), *Myd88*$^{-/-}$, and *Ticam1*$^{-/-}$ demonstrated their sensitivity to the virus (Figure 1D). The analysis of the kinetics of plasma membrane integrity loss revealed that within 10 min after the virus administration, nuclei of all liver macrophages became PI positive (Figure 1E). Ultrastructural analysis of liver macrophages 15 min after the virus challenge revealed catastrophic disorganization of the cytosol and swollen mitochondria (Figures 1F). Administration of HAdv into mice also resulted in a significant increase in the amount of cytosolic enzyme lactate dehydrogenase (LDH) in plasma, compared to the saline-injected group (Figure 1G). Collectively, the ultrastructural changes, along with the loss of the plasma membrane integrity, are consistent with morphological and functional changes associated with necrotic forms of cell death (Ting et al., 2008). However, this necrotic-type cell death occurs with extremely rapid kinetics and independently of the known principal mediators that execute both apoptotic and necrotic cell-death programs (Galluzzi et al., 2012).

Macrophages in *Irf3*$^{-/-}$ Are Resistant to Virus-Induced Necrotic Cell Death

Next, we extended our analyses to mice deficient in mediators of virus infection-sensing pathways. This analysis revealed that in mice deficient in transcriptional factor IRF3 (Sato et al., 2000), liver macrophages were resistant to HAdv-induced cell death (Figures 2A–2C and S2). Furthermore, in *Irf3*$^{-/-}$ mice, CD68$^+$ cells were present in the liver parenchyma even 24 hr after the virus challenge (Figures 2B and 2C). Surprisingly, CD68$^+$ cells in the livers of mice deficient in IPS-1/MAVS/VISA (Kawai et al., 2005; Meylan et al., 2005; Seth et al., 2005; Xu et al., 2005) and STING (Ishikawa and Barber, 2008; Sauer et al., 2011b), which operate upstream of IRF3 in viral genome-sensing pathways, as well as in mice deficient in cytosolic DNA sensor DAI (*Zbp1*$^{-/-}$) (Takaoka et al., 2007), were sensitive to HAdv challenge (Figures 2A and 2B).

Because activation of IRF3 as a transcription activation factor associates with its phosphorylation at Ser396 (Yoneyama et al.,

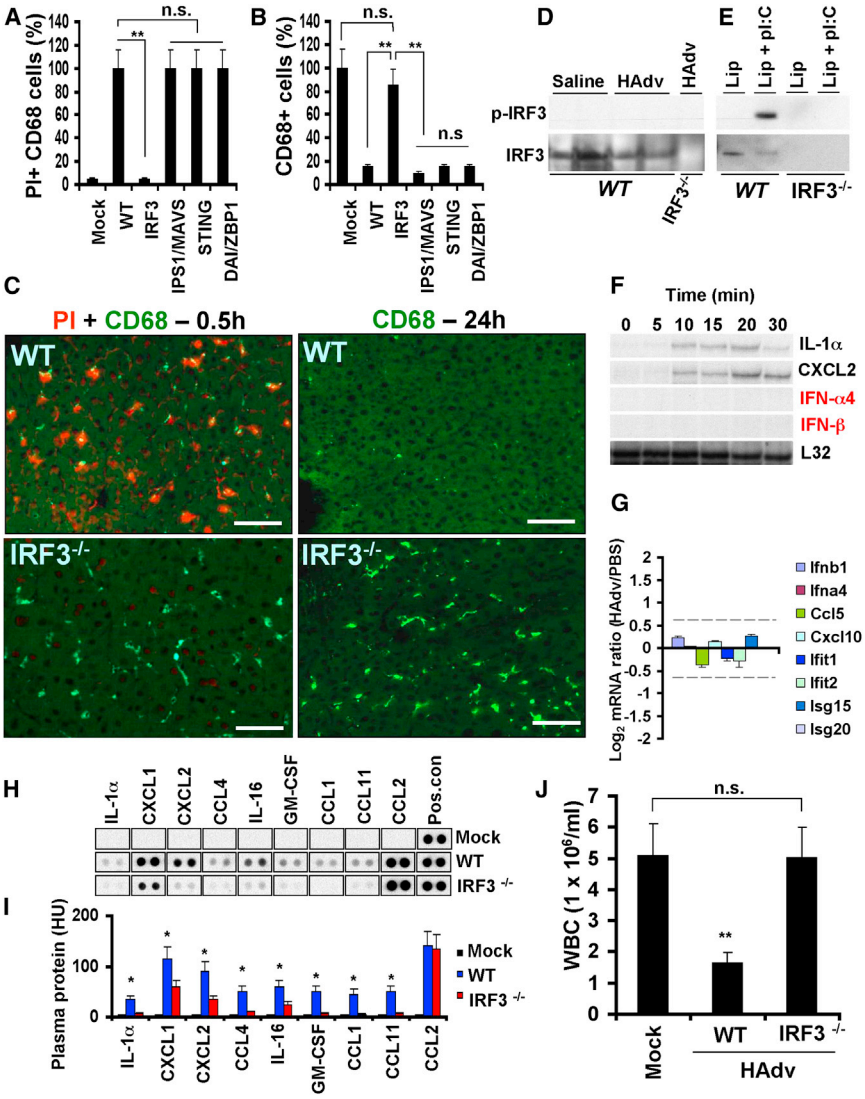

Figure 2. Macrophages in *Irf3*$^{-/-}$, but Not in IPS1/MAVS- or STING-Deficient Mice, Are Resistant to Virus-Induced Necrotic Cell Death

(A and B) The percentage of PI-permeable CD68^{+} cells in the liver parenchyma of indicated gene-deficient mice 1 hr (A) or 24 hr (B) after challenge with HAdv (n = 8). Error bars represent SD of the mean. **p < 0.001. n.s., not statistically significant.

(C) The sections of livers from WT or IRF3$^{-/-}$ mice 0.5 and 24 hr after challenge with HAdv and PI were stained with anti-CD68-mAb (green) and PI (red) analyzed by fluorescent microscopy. Scale bars, 30 μm (n = 6).

(D and E) Western blot analysis of IRF3 phosphorylation at Ser 396 in the livers of mice 20 min after saline or HAdv injection (D) or in the mouse bone marrow-derived macrophages (E) from *WT* and *Irf3*$^{-/-}$ mice treated with either Lipofectamine alone (Lip) or with a mixture of Lipofectamine and poly-I:C.

(F) Kinetics of transcriptional activation of NF-κB-dependent IL-1α, CXCL2, and IRF3-dependent IFN-α4 and IFN-β genes in the liver of mice from 0 to 30 min after intravenous infection with adenovirus, determined by the RNase protection assay (n = 3).

(G) The ratio of the amounts of mRNAs for IRF3-dependent genes in the spleen of *WT* mice 30 min after infection with HAdv versus mice injected with PBS, determined by mRNA arrays. The data for the indicated gene set were extracted from the microarray data set collected earlier and deposited to the Gene Expression Omnibus database under the accession number GSE36078 (n = 3). The 1.5-fold differential expression interval is depicted with dotted lines.

(H) The proinflammatory cytokines and chemokines in plasma of WT and IRF3$^{-/-}$ mice 1 hr after challenge with HAdv, determined by Proteome Profiler antibody array (n = 4). Mock, mice injected with saline; Pos.con., manufacturer's internal positive control samples on each membrane.

(I) Quantitative representation of the dot blot data shown in (H) analyzed by densitometry and histogram processing tool. HU, histogram units.

(J) Total white blood cell (WBC) count in the blood of WT and IRF3$^{-/-}$ mice 24 hr after challenge with HAdv. **p < 0.01 (n = 8).

See also Figure S2.

2002), we analyzed whether IRF3 is phosphorylated at Ser396 by the time of macrophage cell death. Western blot analysis showed that IRF3 became phosphorylated at Ser396 in response to cell treatment with poly-I:C in vitro; however, Ser396 IRF3 phosphorylation was lacking in both saline and HAdv-treated mice (Figures 2D and 2E). The analysis of IRF3-dependent gene expression in the liver and spleen (Figures 2F and 2G) by 30 min after the virus challenge further revealed the lack of transcriptional activation of IRF3-dependent genes.

Necrotic-type cell death associates with systemic inflammatory response syndrome that can be lethal to the host (Kaczmarek et al., 2013). Therefore, we challenged *WT* and *Irf3*$^{-/-}$ mice with HAdv and analyzed plasma cytokines and chemokines 1 hr after virus administration. This analysis showed that numerous proinflammatory cytokines and chemokines, including IL-1α, IL-16, GM-CSF, CCL1, CCL4, CCL11, CXCL1, and CXCL2, were elevated in the plasma of *WT*, but not *Irf3*$^{-/-}$, mice after the virus challenge (Figures 2H and 2I). Consistent with the reduced levels of cytokines and chemokines, cytopenia (a clinical marker of systemic inflammatory response) was not observed in *Irf3*$^{-/-}$ mice after the virus challenge, whereas *WT* mice were highly cytopenic after the virus infection (Figure 2J).

IRF3 Triggers Macrophage Necrosis upon Pathogen Entry into the Cytosol

Earlier analyses suggested that HAdv entry into the cytosol is required for the induction of macrophage cell death in vivo (Smith et al., 2008). However, many viral and bacterial pathogens target cytosol as an effective reproductive niche within the cell. Therefore, we infected mice with wild-type adenovirus serotypes HAdv2, HAdv5, replication-defective adenovirus vector Ad5GFP, or a single-point HAdv2 mutant *ts1*, which cannot

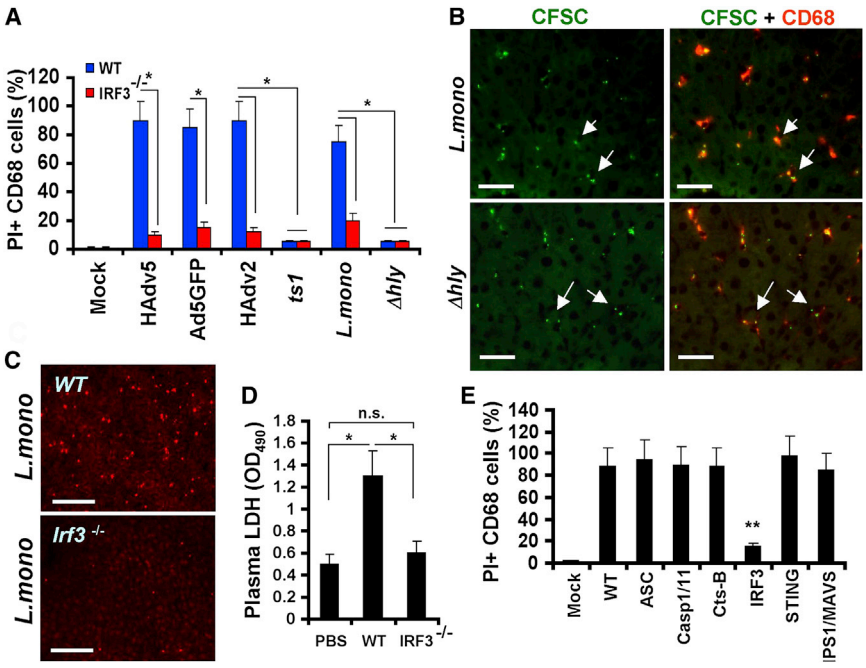

Figure 3. *L. monocytogenes* and HAdv Trigger IRF3-Dependent Macrophage Necrosis In Vivo upon Entry into the Cytosol

(A) The percentage of PI-permeable CD68$^+$ cells in the liver parenchyma of WT and IRF3$^{-/-}$ mice 60 min after challenge with indicated pathogens (n = 6). Error bars represent SD of the mean. *p < 0.01.

(B) Immunofluorescent microscopy analysis of distribution of CFSC-labeled *L. monocytogenes* (*L.mono*) or Δ*hly* cells (green) in liver parenchyma at 30 min postinfection revealed their accumulation in CD68$^+$ resident macrophages (red, indicated by arrows) (n = 8). Scale bars, 20 μm.

(C) Distribution of PI-permeable cells in livers of *WT* and *Irf3*$^{-/-}$ mice 1 hr after *L. monocytogenes* infection (n = 5). Scale bars, 50 μm.

(D) Plasma LDH levels in mice mock infected with saline (PBS) or WT and IRF3$^{-/-}$ mice infected with *L. monocytogenes* 1 hr postinfection (n = 5). *p < 0.01.

(E) The percentage of PI-permeable CD68$^+$ cells in the liver parenchyma of indicated gene-deficient mice 1 hr after challenge with *L. monocytogenes*. Error bars represent SD of the mean (n = 8). Mice were injected with saline in the mock-infected group (Mock). **p < 0.01.

See also Figure S3.

escape from the endosomal compartment into the cytosol (Greber et al., 1993). We also infected mice with wild-type *L. monocytogenes* as a representative facultative cytosolic bacterial pathogen or its isogenic mutant Δ*hly* that lacks Listeriolysin O and fails to escape from the phagosomal compartment into the cytosol (Portnoy et al., 1988). The analysis of the loss of plasma membrane integrity by liver macrophages after *WT* mice infection with all of these pathogens showed that liver macrophages rapidly became PI permeable in response to HAdv2, HAdv5, Ad5GFP vector, and *L. monocytogenes* infection (Figure 3A). However, both the *ts1* adenovirus and Δ*hly* *L. monocytogenes* mutant failed to induce permeability of liver macrophages to PI (Figures 3A and S3). Remarkably, macrophages in *Irf3*$^{-/-}$ mice did not lose plasma membrane integrity after infection with all of these pathogens (Figures 3A–3C and S3). We further confirmed that CD68$^+$ liver macrophages efficiently sequester *L. monocytogenes* from the blood (Figure 3B), and liver macrophage permeability to the PI after *L. monocytogenes* infection associates with elevated LDH levels in plasma in *WT* but not *Irf3*$^{-/-}$ mice, demonstrating that upon entry into macrophages in vivo, *L. monocytogenes* triggers genuine and rapid physiologically regulated necrosis that requires pathogen entry into the cytosol. Similar to results observed with mouse infection with HAdv, we found that liver macrophages became PI permeable after *L. monocytogenes* infection of mice deficient in inflammasome components ASC, caspase-1 and caspase-11, cathepsin-B, STING, and IPS1/MAVS, but not in *Irf3*$^{-/-}$ mice (Figure 3E). Collectively, these data demonstrate that IRF3 triggers necrosis in vivo in response to both HAdv and *L. monocytogenes* infection. Furthermore, pathogen penetration into the cytosol is required to induce this form of necrosis.

IRF3-Dependent "Defensive Suicide" Is a Protective Macrophage Effector Mechanism against Disseminated Virus Infection

To analyze the functional relevance of IRF3-dependent macrophage necrosis for host defense against disseminated infections, we first infected *WT* and *Irf3*$^{-/-}$ mice with *L. monocytogenes* and analyzed pathogen burden in the liver 6 hr postinfection. This analysis showed that the bacterial burden doubled over this time frame, but only in *WT* and not in *Irf3*$^{-/-}$ mice (Figure 4A). In contrast, upon infection of *WT* and *Irf3*$^{-/-}$ mice with wild-type HAdv5, 24 hr postinfection, the pathogen burden was significantly higher in the livers of mice deficient in IRF3, compared to control *WT* mice (Figure 4B).

The observation that macrophages induce IRF3-dependent necrotic death within minutes after interaction with HAdv may indicate that this form of regulated necrosis functionally represents a defensive suicide strategy that must be effective at enabling immunity to disseminated virus infection. Consequently, for the host that lacks this macrophage population, even a sublethal virus infection may lead to compromised resistance and be detrimental to survival. To experimentally evaluate this assumption, we depleted wild-type mice of tissue macrophages with clodronate liposomes prior to their challenge with escalating sublethal doses of the wild-type HAdv5 and compared the virus burden in the liver 48 hr after virus administration. This analysis revealed that in mice depleted of tissue macrophages, there were two to three orders of magnitude higher virus DNA burden compared to mice with liver macrophages intact (Figure 4C). The serum levels of liver enzymes ALT and AST, indicating virus-induced hepatotoxicity, were significantly (up to 10-fold) higher in macrophage-depleted mice, compared to mice with tissue macrophages (Figure 4D). Furthermore,

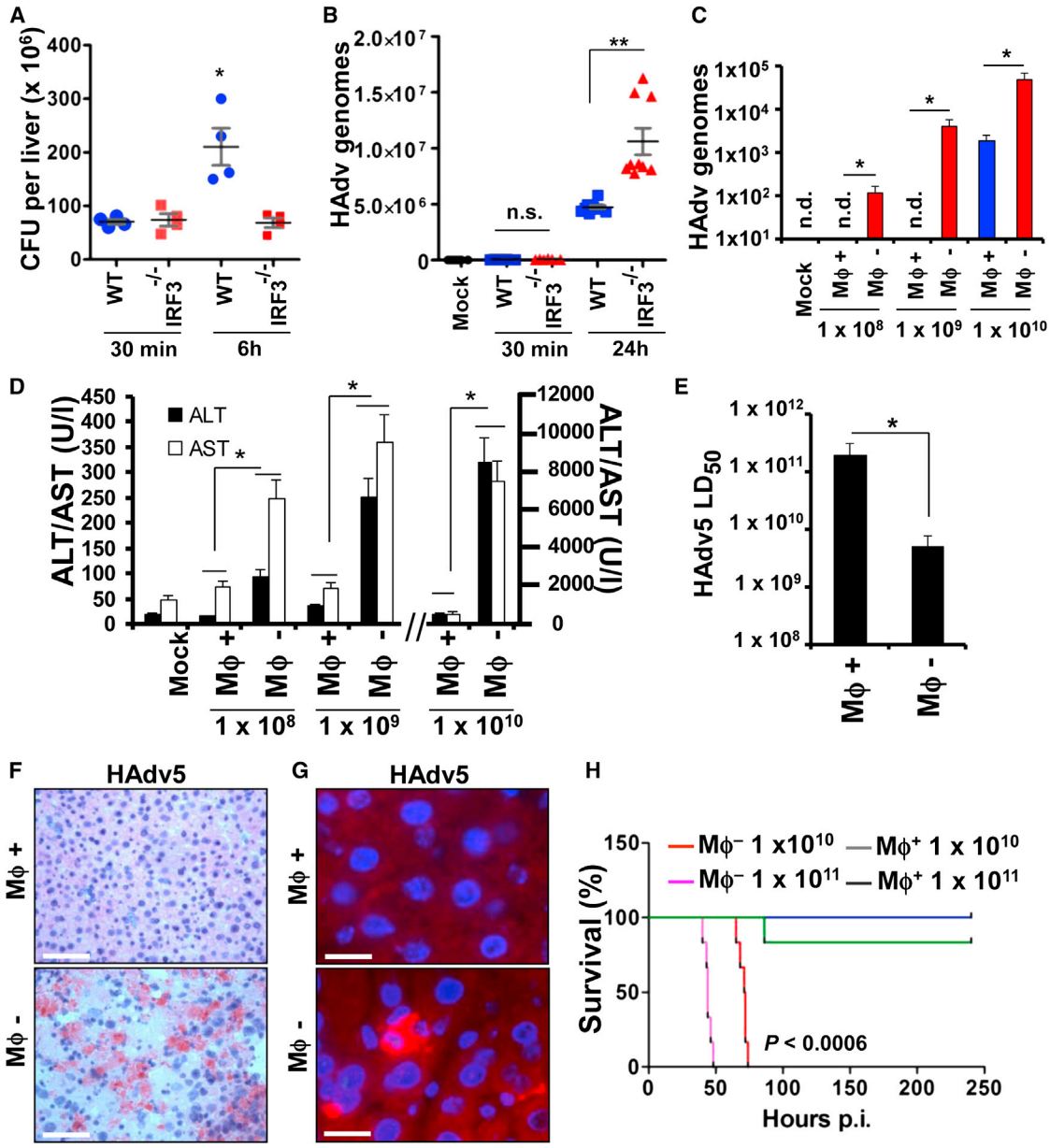

Figure 4. IRF3-Dependent Defensive Suicide Is a Protective Macrophage Effector Mechanism against Disseminated Virus Infection

(A and B) Pathogen burden in the livers of WT and IRF3$^{-/-}$ mice infected with *L. monocytogenes* (A) and wild-type HAdv5 (B) analyzed at indicated times. Representative data from two experiments are shown. The data in (A) were analyzed by one-way ANOVA (*p = 0.0014) and in (B) by one-way ANOVA with post hoc Kruskal-Wallis test (**p < 0.001).

(C) The amounts of the virus genomic DNA in the livers of wild-type mice depleted of tissue macrophages with clodronate liposomes (Mϕ −) or mice containing tissue macrophages (Mϕ +; mice were injected with liposomes containing saline only) 48 hr after challenge with HAdv5 at indicated doses (in virus particles per mouse). The amounts of viral genomes per 10 ng of total liver DNA are shown (n = 6). *p < 0.01. n.d., not determined.

(D) The amounts of liver enzymes ALT and AST in plasma Mϕ− and Mϕ+ mice 48 hr after challenge with HAdv5 at indicated doses. In Mock settings, ALT and AST levels were similar in Mϕ+ and Mϕ− mice prior to virus challenge (n = 6). *p < 0.01.

(E) Reduction of LD_{50} of HAdv5 for mice after depletion of tissue macrophages with clodronate liposomes (Mϕ−), compared to mice containing tissue macrophages (Mϕ+) (n = 9). *p < 0.05.

(F) Hematoxylin and eosin staining of liver sections from Mϕ+ and Mϕ− mice 48 hr after infection with 10^{10} virus particles of HAdv5. Scale bars, 100 μm.

(G) Sections of liver as in (F) after staining with anti-HAdv5 hexon Ab (red). Cell nuclei were counterstained with DAPI (blue). Scale bars, 10 μm.

(H) Survival of Mϕ− and Mϕ+ mice after challenge with indicated doses of HAd5 (n = 8). Statistical significance of p < 0.0006 is indicated for groups of Mϕ− mice when compared to Mϕ+ mice using log rank test. Hours p.i., hours postinfection.

depletion of tissue macrophages from mice resulted in over 10-fold reduction in LD_{50}, extensive histologically evident liver damage, virus replication, and protein expression (Figures 4E–4G). At sublethal doses of 10^{10} and 10^{11} virus particles per mouse, the majority of macrophage-containing mice survived the infection for the duration of the experiment (250 hr postvirus infection), whereas 100% of macrophage-depleted mice succumbed by 75 hr ($p < 0.0006$) (Figure 4H). Collectively, these data provide experimental evidence that HAdv-triggered macrophage cell death effectively reduces the virus burden and protects the host from sublethal doses of disseminated virus in vivo.

DISCUSSION

In this study, we implicated IRF3 as a critical and nonredundant factor required for the execution of a necrotic cell-death type that ensues in response to viral and bacterial pathogens. We found that upon triggering necrotic death, IRF3 does not function as a transcription-activating factor. Although IRF3 can be activated downstream of the IPS1/MAVS/VISA- and STING-mediated viral genome-sensing pathway as well as TBK1/IKKε signaling in various cell types (Fitzgerald et al., 2003; Takeuchi and Akira, 2009), our data indicate that in the context of IRF3-dependent necrosis, both IPS1/MAVS and STING, as well as BAK and BAX (Chattopadhyay et al., 2010, 2011), are all dispensable for the induction and execution of cell death in vivo. Using the entire genetic evidence in mice deficient in cathepsin-B, inflammasome component ASC (which is required for NLRP3-mediated inflammasome activation), caspases 1 and 11, as well as ROS-producing NADPH-oxidase components $p47^{Phox}$ and $gp91^{Phox}$, we found that liver macrophages rapidly lose their plasma membrane integrity after HAdv infection, indicating that IRF3-dependent necrosis is a distinct pathway and requires none of these components to ensue in vivo.

Caspase-1-dependent pyroptosis is an important host defense mechanism and constitutes a necrotic-type cell death that ablates the niche for pathogen replication (Bergsbaken et al., 2009). However, pyroptosis per se does not result in the reduction of pathogen burden, and to control the infection, bacteria released from pyroptotic cells in vivo are killed by bactericidal effectors produced by the host's neutrophils (Miao et al., 2010). Here, we showed that the induction of IRF3-dependent necrosis in vivo does not result in the reduction of *L. monocytogenes* burden in the liver, but rather, it supports the infection. It is noteworthy that *L. monocytogenes* that was engineered to ectopically express *Legionella pneumophila* flagellin and, therefore, became highly efficient at activating NLRC4 inflammasome, in vivo exhibited a severely attenuated phenotype, compared to the parental *L. monocytogenes* strain (Sauer et al., 2011a). Together, these data suggest that bacterial pathogens may have evolved specific mechanisms to activate proinflammatory necrotic-type cell death in vivo to propagate the infection, likely via the recruitment of pathogen-susceptible monocytes. However, a delicate balance may exist where an excessive or untimely proinflammatory cell death limits pathogen survival.

The unique feature of the IRF3-dependent necrosis is its extremely rapid kinetics that enables host protection from disseminated virus infection. RIPK1-RIPK3-dependent necroptosis was shown to play a key role in development and immunity (Declercq et al., 2009; Green et al., 2011). However, in response to physiological stimuli, necroptosis occurs with much slower kinetics and was shown to be targeted by specific viral genes to prevent cell-death execution (Upton et al., 2010, 2012). Our finding of IRF3-dependent cell death may also be relevant to conditions and pathologies beyond host responses to disseminated infections with viral and bacterial pathogens. The development of specific pharmacological inhibitors of this regulated necrotic cell-death type may reveal its contribution and be found useful for the treatment of inflammatory diseases and conditions where underlying pathology is associated with perpetual cycles of proinflammatory cell death.

EXPERIMENTAL PROCEDURES

All animal studies were carried out with the approval of the Institutional Animal Care and Use Committee of the University of Washington, Seattle. C57BL/6 mice were purchased from Charles River Laboratories. All mice were on C57BL/6 genetic background, matched by age, and housed in specific pathogen-free facilities. Mice were infected with wild-type HAdv at a dose of 1×10^{10} virus particles per mouse via tail vein infusion. Viral particle titers were determined by OD_{260} measurement. For in vivo experiments, only virus preparations confirmed to be free of endotoxin contamination were used. *L. monocytogenes* and isogenic Δ*hly* strains were grown on BHI plates from frozen stocks. Stationary cultures were initiated from single colonies and incubated at 30°C overnight. Two to 4 hr prior to bacteria administration into mice at a dose of 10^8 cfu via the tail vein infusion, fresh cultures were initiated and incubated at 37°C with shaking as described in Sauer et al. (2011a). Bacteria titers were measured by optical density and verified by plating serial 10-fold dilutions on BHI plates. Administration of this dose of *L. monocytogenes* into the bloodstream resulted in deposition of one to two visible bacterial cells per liver macrophage (determined by injecting CFSC-labeled bacteria). Proteome Profiler antibody array "Mouse Cytokine Array Panel A" (#ARY006) was from R&D Systems and was used according to the manufacturer's instructions. Unless otherwise noted, statistical analysis in each independent experiment was performed with an unpaired, two-tailed Student's t test. Data are reported as mean ± SD. A p value <0.05 was considered statistically significant. Animal survival was analyzed using log rank test and GraphPad Prism 5 software. See Extended Experimental Procedures for more information.

SUPPLEMENTAL INFORMATION

Supplemental Information includes Extended Experimental Procedures, three figures, and one table and can be found with this article online at http://dx.doi.org/10.1016/j.celrep.2013.05.025.

LICENSING INFORMATION

ACKNOWLEDGMENTS

We thank Drs. V. Dixit (Roche) for *Pycard*$^{-/-}$ and *Ripk3*$^{-/-}$, R.A. Flavell (Yale University) for *Casp1/11*$^{-/-}$, S. Akira (Osaka University) for *Myd88*$^{-/-}$, *Tlr4*$^{-/-}$, *Tlr7/8*$^{-/-}$, *Tlr9*$^{-/-}$, and *Zbp1*$^{-/-}$, R. Vance (University of California, Berkeley) for *Tmem173*$^{Gt/Gt}$, M. Gale, Jr. (University of Washington) for *Sti*$^{-/-}$ (*Mavs*$^{-/-}$), R. Hakem (University of Toronto) for *Casp8*$^{fl/fl}$, S. Hedrick (University of California, San Diego) for *Casp8*$^{fl/fl}$, D. Green (St. Jude Children's Research Hospital) for *Casp8*$^{-/-}$*Ripk3*$^{-/-}$, T. Mak (University Health Network) for *Cradd*$^{-/-}$,

T. Reinheckel (Albert-Ludwigs-University Freiburg) and J. Joyce (Memorial Sloan-Kettering Cancer Center) for *Ctsb*$^{-/-}$, *Ctss*$^{-/-}$, and *Ctsl*$^{-/-}$, Y. Iwakura (University of Tokyo) for *Il1a*$^{-/-}$ and *Il1a/b*$^{-/-}$, D. Chaplin (University of Alabama) for *Il1b*$^{-/-}$, M. Wewers (Ohio State University) for *Il1b*$^{-/-}$/*Il18*$^{-/-}$, and T. Taniguchi (University of Tokyo) for *Irf3*$^{-/-}$ mice. We are thankful to A. Byrnes (US Food and Drug Administration) for providing *ts1* virus. *L. monocytogenes* (10403S) and isogenic Δ*hly* strains were provided by E. Miao (University of North Carolina, Chapel Hill) and A. Aderem (SeattleBiomed). This study was supported by US NIH grants AI065429 and CA141439 to D.M.S.

Received: January 9, 2013
Revised: April 15, 2013
Accepted: May 13, 2013
Published: June 13, 2013

REFERENCES

Bergsbaken, T., Fink, S.L., and Cookson, B.T. (2009). Pyroptosis: host cell death and inflammation. Nat. Rev. Microbiol. *7*, 99–109.

Chattopadhyay, S., Marques, J.T., Yamashita, M., Peters, K.L., Smith, K., Desai, A., Williams, B.R.G., and Sen, G.C. (2010). Viral apoptosis is induced by IRF-3-mediated activation of Bax. EMBO J. *29*, 1762–1773.

Chattopadhyay, S., Yamashita, M., Zhang, Y., and Sen, G.C. (2011). The IRF-3/Bax-mediated apoptotic pathway, activated by viral cytoplasmic RNA and DNA, inhibits virus replication. J. Virol. *85*, 3708–3716.

Declercq, W., Vanden Berghe, T., and Vandenabeele, P. (2009). RIP kinases at the crossroads of cell death and survival. Cell *138*, 229–232.

Fitzgerald, K.A., McWhirter, S.M., Faia, K.L., Rowe, D.C., Latz, E., Golenbock, D.T., Coyle, A.J., Liao, S.M., and Maniatis, T. (2003). IKKepsilon and TBK1 are essential components of the IRF3 signaling pathway. Nat. Immunol. *4*, 491–496.

Galluzzi, L., Vitale, I., Abrams, J.M., Alnemri, E.S., Baehrecke, E.H., Blagosklonny, M.V., Dawson, T.M., Dawson, V.L., El-Deiry, W.S., Fulda, S., et al. (2012). Molecular definitions of cell death subroutines: recommendations of the Nomenclature Committee on Cell Death 2012. Cell Death Differ. *19*, 107–120.

Greber, U.F., Willetts, M., Webster, P., and Helenius, A. (1993). Stepwise dismantling of adenovirus 2 during entry into cells. Cell *75*, 477–486.

Green, D.R., Oberst, A., Dillon, C.P., Weinlich, R., and Salvesen, G.S. (2011). RIPK-dependent necrosis and its regulation by caspases: a mystery in five acts. Mol. Cell *44*, 9–16.

Ishikawa, H., and Barber, G.N. (2008). STING is an endoplasmic reticulum adaptor that facilitates innate immune signalling. Nature *455*, 674–678.

Kaczmarek, A., Vandenabeele, P., and Krysko, D.V. (2013). Necroptosis: the release of damage-associated molecular patterns and its physiological relevance. Immunity *38*, 209–223.

Kawai, T., Takahashi, K., Sato, S., Coban, C., Kumar, H., Kato, H., Ishii, K.J., Takeuchi, O., and Akira, S. (2005). IPS-1, an adaptor triggering RIG-I- and Mda5-mediated type I interferon induction. Nat. Immunol. *6*, 981–988.

Kojaoghlanian, T., Flomenberg, P., and Horwitz, M.S. (2003). The impact of adenovirus infection on the immunocompromised host. Rev. Med. Virol. *13*, 155–171.

Lieber, A., He, C.Y., Meuse, L., Schowalter, D., Kirillova, I., Winther, B., and Kay, M.A. (1997). The role of Kupffer cell activation and viral gene expression in early liver toxicity after infusion of recombinant adenovirus vectors. J. Virol. *71*, 8798–8807.

Manickan, E., Smith, J.S., Tian, J., Eggerman, T.L., Lozier, J.N., Muller, J., and Byrnes, A.P. (2006). Rapid Kupffer cell death after intravenous injection of adenovirus vectors. Mol. Ther. *13*, 108–117.

Meylan, E., Curran, J., Hofmann, K., Moradpour, D., Binder, M., Bartenschlager, R., and Tschopp, J. (2005). Cardif is an adaptor protein in the RIG-I antiviral pathway and is targeted by hepatitis C virus. Nature *437*, 1167–1172.

Miao, E.A., Leaf, I.A., Treuting, P.M., Mao, D.P., Dors, M., Sarkar, A., Warren, S.E., Wewers, M.D., and Aderem, A. (2010). Caspase-1-induced pyroptosis is an innate immune effector mechanism against intracellular bacteria. Nat. Immunol. *11*, 1136–1142.

Morral, N., O'Neal, W.K., Rice, K., Leland, M.M., Piedra, P.A., Aguilar-Córdova, E., Carey, K.D., Beaudet, A.L., and Langston, C. (2002). Lethal toxicity, severe endothelial injury, and a threshold effect with high doses of an adenoviral vector in baboons. Hum. Gene Ther. *13*, 143–154.

Portnoy, D.A., Jacks, P.S., and Hinrichs, D.J. (1988). Role of hemolysin for the intracellular growth of *Listeria monocytogenes*. J. Exp. Med. *167*, 1459–1471.

Sato, M., Suemori, H., Hata, N., Asagiri, M., Ogasawara, K., Nakao, K., Nakaya, T., Katsuki, M., Noguchi, S., Tanaka, N., and Taniguchi, T. (2000). Distinct and essential roles of transcription factors IRF-3 and IRF-7 in response to viruses for IFN-alpha/beta gene induction. Immunity *13*, 539–548.

Sauer, J.D., Pereyre, S., Archer, K.A., Burke, T.P., Hanson, B., Lauer, P., and Portnoy, D.A. (2011a). *Listeria monocytogenes* engineered to activate the Nlrc4 inflammasome are severely attenuated and are poor inducers of protective immunity. Proc. Natl. Acad. Sci. USA *108*, 12419–12424.

Sauer, J.D., Sotelo-Troha, K., von Moltke, J., Monroe, K.M., Rae, C.S., Brubaker, S.W., Hyodo, M., Hayakawa, Y., Woodward, J.J., Portnoy, D.A., and Vance, R.E. (2011b). The N-ethyl-N-nitrosourea-induced Goldenticket mouse mutant reveals an essential function of Sting in the in vivo interferon response to *Listeria monocytogenes* and cyclic dinucleotides. Infect. Immun. *79*, 688–694.

Seth, R.B., Sun, L.J., Ea, C.K., and Chen, Z.J.J. (2005). Identification and characterization of MAVS, a mitochondrial antiviral signaling protein that activates NF-kappaB and IRF 3. Cell *122*, 669–682.

Smith, J.S., Xu, Z.L., Tian, J., Stevenson, S.C., and Byrnes, A.P. (2008). Interaction of systemically delivered adenovirus vectors with Kupffer cells in mouse liver. Hum. Gene Ther. *19*, 547–554.

Takaoka, A., Wang, Z., Choi, M.K., Yanai, H., Negishi, H., Ban, T., Lu, Y., Miyagishi, M., Kodama, T., Honda, K., et al. (2007). DAI (DLM-1/ZBP1) is a cytosolic DNA sensor and an activator of innate immune response. Nature *448*, 501–505.

Takeuchi, O., and Akira, S. (2009). Innate immunity to virus infection. Immunol. Rev. *227*, 75–86.

Ting, J.P., Willingham, S.B., and Bergstralh, D.T. (2008). NLRs at the intersection of cell death and immunity. Nat. Rev. Immunol. *8*, 372–379.

Upton, J.W., Kaiser, W.J., and Mocarski, E.S. (2010). Virus inhibition of RIP3-dependent necrosis. Cell Host Microbe *7*, 302–313.

Upton, J.W., Kaiser, W.J., and Mocarski, E.S. (2012). DAI/ZBP1/DLM-1 complexes with RIP3 to mediate virus-induced programmed necrosis that is targeted by murine cytomegalovirus vIRA. Cell Host Microbe *11*, 290–297.

Xu, L.G., Wang, Y.Y., Han, K.J., Li, L.Y., Zhai, Z.H., and Shu, H.B. (2005). VISA is an adapter protein required for virus-triggered IFN-beta signaling. Mol. Cell *19*, 727–740.

Yoneyama, M., Suhara, W., and Fujita, T. (2002). Control of IRF-3 activation by phosphorylation. J. Interferon Cytokine Res. *22*, 73–76.